

HIGH-RESOLUTION 3D SIMULATIONS OF RELATIVISTIC JETS

M.A. Aloy ¹, J.M^a Ibáñez ¹, J.M^a Martí ¹, J.L. Gómez ² and E. Müller ³

Received _____; accepted _____

arXiv:astro-ph/9906428v1 26 Jun 1999

¹Departamento de Astronomía y Astrofísica, Universidad de Valencia, 46100 Burjassot (Valencia), Spain

²Instituto de Astrofísica de Andalucía (CSIC) Granada, Spain

³Max-Planck-Institut für Astrophysik, Karl-Schwarzschild-Str.1, 85748 Garching, Germany

ABSTRACT

We have performed high-resolution 3D simulations of relativistic jets with beam flow Lorentz factors up to 7, a spatial resolution of 8 cells per beam radius, and for up to 75 normalized time units to study the morphology and dynamics of 3D relativistic jets. Our simulations show that the coherent fast backflows found in axisymmetric models are not present in 3D models. We further find that when the jet is exposed to non-axisymmetric perturbations, (i) it does not display the strong perturbations found for 3D classical hydrodynamic and MHD jets (at least during the period of time covered by our simulations), and (ii) it does propagate according to the 1D estimate. Small 3D effects in the relativistic beam give rise to a lumpy distribution of apparent speeds like that observed in M87. The beam is surrounded by a boundary layer of high specific internal energy. The properties of this layer are briefly discussed.

Subject headings: galaxies: jets — hydrodynamics — methods: numerical — relativity

1. Introduction

Since several years the dynamical and morphological properties of axisymmetric relativistic jets are investigated by means of relativistic hydrodynamic simulations (van Putten 1993; Duncan & Hughes 1994; Martí *et al.* 1994, 1995, 1997; Komissarov & Falle 1998; Rosen *et al.* 1999). In addition, relativistic MHD simulations have been performed in 2D (Koide, Nishikawa & Muttel 1996; Koide 1997) and 3D (Nishikawa *et al.* 1997, 1998). In their 3D simulations Nishikawa *et al.* have studied mildly relativistic jets (Lorentz factor 4.56) propagating both along and obliquely to an ambient magnetic field. In this Letter we report on high-resolution 3D simulations of relativistic jets with the largest beam flow Lorentz factor performed up to now (7.09), the largest resolution (8 cells per beam radius), and covering the longest time evolution (75 normalized time units; a normalized time unit is defined as the time needed for the jet to cross a unit length; see Massaglia, Bodo & Ferrari 1996).

The calculations have been performed with the high-resolution 3D relativistic hydrodynamics code GENESIS (Aloy *et al.* 1999), which is an upgraded version of the code developed by Martí, Müller & Ibáñez (1994) and Martí *et al.* (1995). GENESIS integrates the 3D relativistic hydrodynamic equations in conservation form in Cartesian coordinates including an additional conservation equation for the density of beam material. The computations were performed on a Cartesian domain (X,Y,Z) of size $15R_b \times 15R_b \times 75R_b$ ($120 \times 120 \times 600$ computational cells), where R_b is the beam radius. The jet is injected at $z = 0$ along the positive z -axis through a circular nozzle defined by $x^2 + y^2 \leq R_b^2$. Beam material is injected with a beam mass fraction $f = 1$, and the computational domain is initially filled with an external medium ($f = 0$).

We have considered a 3D model corresponding to model C2 of Martí *et al.* (1997), which is characterized by a beam-to-external proper rest-mass density ratio $\eta = 0.01$, a

beam Mach number $M_b = 6.0$, and a beam flow speed $v_b = 0.99c$ (c is the speed of light) or a beam Lorentz factor $W_b \approx 7.09$. An ideal gas equation of state with an adiabatic exponent $\gamma = 5/3$ is assumed to describe both the jet matter and the ambient gas. The beam is assumed to be in pressure equilibrium with the ambient medium.

The evolution of the jet was simulated up to $T \approx 150R_b/c$, when the head of the jet is about to leave the grid. The mean jet propagation speed $v_h \approx 0.5c$, while the 1D estimate of the jet propagation speed (see, *e.g.*, Martí *et al.* 1997) gives $0.42c$, *i.e.*, our simulations are still within the 1D phase (see Martí, Müller & Ibáñez 1998).

Non-axisymmetry was imposed by means of a helical velocity perturbation at the nozzle given by

$$v_b^x = \zeta v_b \cos\left(\frac{2\pi t}{\tau}\right), \quad v_b^y = \zeta v_b \sin\left(\frac{2\pi t}{\tau}\right), \quad v_b^z = v_b \sqrt{1 - \zeta^2}, \quad (1)$$

where ζ is the ratio of the toroidal to total velocity and τ the perturbation period (*i.e.*, $\tau = T/n$, n being the number of cycles completed during the whole simulation). The wavelength of the perturbation, λ , is obtained from the expression $\lambda = v_b^z \tau \approx \frac{v_b L}{v_h n}$, where L is the axial dimension of the grid.

2. Morphology and dynamics of 3D relativistic jets

We have considered a model with a 1% perturbation in helical velocity ($\zeta = 0.01$) and $n = 50$. Figure 1 shows various quantities of the jet in the plane $y = 0$ at the end of the simulation. Two values of the beam mass fraction are marked by white contour levels. The beam structure is dominated by the imposed helical pattern with a characteristic wavelength of $\approx 3.0R_b$ (to be compared with the value $\lambda = 3.5R_b$ expected from the estimate of λ in the previous paragraph) and an amplitude of $\approx 0.2R_b$.

2.1. Cocoon

The overall jet’s morphology is characterized by the presence of a highly turbulent, subsonic, asymmetric cocoon. The pressure distribution outside the beam is nearly homogeneous giving rise to a symmetric bow shock (Fig. 1b). As in the classical case (Norman 1996), our relativistic 3D simulation shows less ordered structures in the cocoon. The cocoon remains quite thin ($\sim 2R_b$) as long as the jet propagates efficiently.

The flow field outside the beam shows that the high velocity backflow is restricted to a small region in the vicinity of the hot spot (Fig. 1e), the largest backflow velocities ($\sim 0.5c$) being significantly smaller than in 2D models. The flow with high Lorentz factor found in axisymmetric simulations (see flow patterns in Martí *et al.* 1996) appears here restricted to a thin layer around the beam and possesses sub-relativistic speeds ($\sim 0.25c$). The magnitude of the backflow velocities in the cocoon do not support relativistic beaming.

2.2. Beam and hot spot

Within the beam the perturbation pattern is superimposed to the conical shocks at about 26 and 50 R_b . The beam does not exhibit the strong perturbations (deflection, twisting, flattening or even filamentation) found by other authors (Norman (1996) for 3D classical hydrodynamic jets; Hardee (1996) for 3D classical MHD jets). This can be taken as a sign of stability, although it can be argued that our simulation is not evolved far enough. Obviously, the beam cross section and the internal conical shock structure are correlated (bottom panel in Figure 1). Before the first recollimation shock the beam cross section shrinks to an effective radius of $0.7R_b$. After this shock and in the rarefaction the beam reexpands and stretches due to an elliptical surface mode (e.g., Hardee 1996). Between $37R_b \lesssim z \lesssim 50R_b$ the beam flow is influenced by the second recollimation shock, which causes

a compression of the beam. A triangular mode seems to grow in this region.

The helical pattern propagates along the jet at nearly the beam speed (see animation at <http://scry.uv.es/aloy.html/JETS/videos/n50p01>) which could yield to superluminal components when viewed at appropriate angles. Besides this superluminal pattern, the presence of emitting fluid elements moving at different velocities and orientations could lead to local variations of the apparent superluminal motion within the jet. This is shown in Fig. 2, where we have computed the mean (along each line of sight, and for a viewing angle of 40 degrees) local apparent speed. The distribution of apparent motions is inhomogeneous and resembles that of the observed individual features within knots in M87 (Biretta, Zhou, & Owen 1995).

The jet can be traced continuously up to the hot spot which propagates as a strong shock through the ambient medium. Beam material impinges on the hot spot at high Lorentz factors. We could not identify a terminal Mach disk in the flow. We find flow speeds near (and in) the hot spot much larger than those inferred from the one dimensional estimate. This fact was already noticed for 2D models by Komissarov & Falle (1996) and suggested by them as a plausible explanation for an excess in hot spot beaming.

2.3. Beam/cocoon shear layer

We find a layer of high specific internal energy (Fig. 1d) surrounding the beam like in previous axisymmetric models (Aloy *et al.* 1999). A comparison with the backflow velocities (Fig. 1e) shows that it is mainly composed of forward moving beam material at a speed smaller than the beam speed. The intermediate speed of the layer material is due to shear in the beam/cocoon interface, which is also responsible for its high specific internal energy. The existence of such a boundary layer has been invoked by several authors (Komissarov

1990, Laing 1996) to interpret a number of observational trends in FRI radio sources. Swain, Bridle & Baum (1998) have found evidence for these boundary layers in FRIIs (3C353).

The diffusion of vorticity caused by numerical viscosity is responsible for the formation of the boundary layer. Although being caused by numerical effects (and not by the physical mechanism of turbulent shear) the properties of PPM-based difference schemes are such that they can mimic turbulent flow to a certain degree (Porter & Woodward 1994). Hence, our calculations represent a first approach to study the development of shear layers in relativistic jets and their observable consequences. The structure of both the shear layer and the beam core are sketched in Fig 3. The specific internal energy of the gas in the shear layer (region with $0.2 < f < 0.8$) is typically more than one order of magnitude larger than that of the gas in the beam core. The shear layer broadens with distance from $0.2R_b$ near the nozzle to $1.1R_b$ near the head of the jet (Fig. 4).

2.4. Jet propagation efficiency and disruption

From the head’s position at the end of the simulation ($T = 140.8$) a mean jet advance speed of $0.47c$ is obtained, but the jet’s propagation proceeds in two distinct phases: (i) for $t \lesssim 100$ the jet propagates roughly at the estimated 1D speed ($0.42c$); (ii) for $t \gtrsim 100$ the jet accelerates and propagates at a considerably larger speed ($0.55c$). Comparing with the 3D simulation of Norman (1996) we find a similar behaviour: after a short 1D phase and before the deceleration, the jet transiently accelerates to a propagation speed which is $\approx 20\%$ larger than the corresponding 1D estimate. This result contradicts the one obtained by Nishikawa *et al.* (1997, 1998), who found a propagation speed of only 70% of the corresponding 1D estimate in a shorter (≈ 20 normalized time units) simulation of a denser jet. Although the estimate do not take into account the effect of an extra magnetic pressure in the external

medium opposing to the jet propagation, in the case of Nishikawa *et al.* simulations this magnetic pressure is negligible in comparison with the beam momentum density.

Figure 4 shows the axial component of the momentum of the beam particles (integrated across the beam) along the axis, which decreases by 30% within the first $60 R_b$. Neglecting pressure and viscous effects, and assuming stationarity the axial momentum should be conserved, and hence the beam flow is decelerating. The momentum loss goes along with the growth of the boundary layer whose material is accelerated and heated by viscous stresses. Biconical shocks in the beam are responsible for the break in the axial momentum profiles at $z = 26R_b$ and $z = 50R_b$, because when the beam material passes a conical shock and enters into the adjacent rarefaction fan, it is accelerated by local pressure gradients.

How can the jet accelerate while the beam material is decelerating? Although the beam material decelerates, its terminal Lorentz factor is still large enough to produce a fast jet propagation. On the other hand, in 3D, the beam is prone to strong perturbations which can affect the jet’s head structure. In particular, a simple structure like a terminal Mach shock will probably not survive when significant 3D effects develop. It will be substituted by more complex structures in that case, *e.g.*, by a Mach shock which is no longer normal to the beam flow and which wobbles around the instantaneous flow direction. Another possibility is the generation of oblique shocks near the jet head due to off-axis oscillations of the beam. Although difficult to check quantitatively (due to both the lack of an operative definition for Mach disk identification and the present resolution of our simulations) both possibilities will cause a less efficient deceleration of the beam flow at least during some epochs. At longer time scales the growth of 3D perturbations will cause the beam to spread its momentum over a much larger area than that it had initially, which will efficiently reduce the jet advance speed.

3. Conclusions

We have presented a first attempt to analyze the morpho-dynamical properties of 3D relativistic jets. From our simulations, we can conclude that the coherent fast backflows found in axisymmetric models are not present in 3D models. We have investigated the beam's response to non-axisymmetric perturbations to check its stability. During the period of time studied by us ($t \lesssim 150 R_b/c$), the beam does not display the strong perturbations found by other authors in classical jets (Norman 1996, Hardee 1996) and propagates according to the 1D estimate. Small 3D effects in the relativistic beam give rise to a lumpy distribution of apparent speeds like that observed in M87 (Biretta, Zhou & Owen 1995). We have also analyzed the properties of the boundary layer present in our model.

Obviously, our study must be extended to a wider range of models and perturbations. In particular, stronger perturbations should be considered to reach the nonlinear regime and to identify the acoustic and mixing phases (Bodo 1998) leading to the jet disruption. Further investigation also requires the dependence of the shear layer properties on the perturbation parameters. Finally, appropriate perturbations can be studied that mimic the wiggles observed in specific sources both at pc (0836+710, Lobanov *et al.* 1998; 0735+178, Gómez *et al.* 1999) and kpc scales (M87; Biretta, Zhou & Owen 1995).

ACKNOWLEDGEMENTS

This work has been supported in part by the Spanish DGES (grants PB97-1164 and PB97-1432) and the CSIC-Max Planck Gesellschaft agreement. MAA expresses his gratitude to the Conselleria d'Educació i Ciència de la Generalitat Valenciana for a fellowship. The calculations were carried out on two SGI Origin 2000 at the Centre Europeu de Paral·lelisme de Barcelona and at the Centre de Informàtica de la Universitat de València.

REFERENCES

- Aloy, M.A., Ibáñez, J.M^a., Martí, J.M^a. & Müller, E. 1999, ApJS, in press
- Biretta, J.A., Zhou, F., & Owen, F.N. 1995, ApJ, 447, 582
- Bodo, G., 1998, in *Astrophysical jets: Open problems*, eds. S. Massaglia & G. Bodo, Gordon and Breach, p.161
- Duncan, G.C., & Hughes, P.A. 1994, ApJ, 436, L119
- Gómez, J.L., Marscher, A.P., Alberdi, A., & Gabuzda, D.C. 1999, ApJ, in press
- Hardee, P.E. 1996, in *Energy Transport in Radio Galaxies and Quasars*, eds. P.E. Hardee, A.H. Bridle, J.A. Zensus. ASP Conference Series, Vol. 100, p. 273
- Koide, S. 1997, ApJ, 487, 66
- Koide, S., Nishikawa, K.-I., & Muttel, R.L. 1996, ApJ, 463, L71
- Komissarov, S.S. 1990, Sov. Astron. Lett. 16(4), 284
- Komissarov, S.S., & Falle, S.A.E.G. 1996, in *Energy Transport in Radio Galaxies and Quasars*, eds. P.E. Hardee, A.H. Bridle, J.A. Zensus. ASP Conference Series, Vol. 100, p. 327
- Komissarov, S.S., & Falle, S.A.E.G. 1998, MNRAS, 297, 1087
- Laing, R.A. 1996, in *Energy Transport in Radio Galaxies and Quasars*, eds. P.E. Hardee, A.H. Bridle, J.A. Zensus. ASP Conference Series, Vol. 100, p. 241
- Lobanov, A.P., Krichbaum, T.P., Witzel, A., Kraus, A., Zensus, J.A., Britzen, S., Otterbein, K., Hummel, C.A., & Johnston, K. 1998, A&A, 340, L60

- Martí, J.M^a., Font, J.A., Ibáñez, J.M^a. & Müller, E. 1996, in *Energy Transport in Radio Galaxies and Quasars*, eds. P.E. Hardee, A.H. Bridle, J.A. Zensus. ASP Conference Series, Vol. 100, p. 149
- Martí, J.M^a., Müller, E., Font, J.A., & Ibáñez, J.M^a 1995, *ApJ*, 448, L105
- Martí, J.M^a., Müller, E., Font, J.A., Ibáñez, J.M^a. & Marquina, A. 1997, *ApJ*, 479, 151
- Martí, J. M^a., Müller, E., & Ibáñez, J. M^a 1994, *A&A*, 281, L9
- Martí, J.M^a., Müller, E. & Ibáñez, J.M^a. 1998, in *Astrophysical jets: Open problems*, eds. S. Massaglia & G. Bodo, Gordon and Breach, p.149
- Massaglia, S., Bodo, G., & Ferrari, A. 1996, *A&A*, 307, 997
- Nishikawa, K.–I., Koide, S., Sakai, J., Christodoulou, D.M., Sol, H., & Mutel, R.L. 1997, *ApJ*, 483, L45
- Nishikawa, K.–I., Koide, S., Sakai, J., Christodoulou, D.M., Sol, H., & Mutel, R.L. 1998, *ApJ*, 498, 166
- Norman, M.A. 1996, in *Energy Transport in Radio Galaxies and Quasars*, eds. P.E. Hardee, A.H. Bridle, J.A. Zensus. ASP Conference Series, Vol. 100, p. 319
- Porter, D.H. & Woodward, P.R. 1994, *ApJS*, 93, 309
- Rosen, A., Hughes, P. A., Duncan, G. C., & Hardee, P. E. 1999, *AJ*, in press
- Swain, M.R., Bridle, A.H., & Baum, S.A. 1998, *ApJ*, 507, L29
- van Putten, M.H.P.M. 1993, *ApJ*, 408, L21

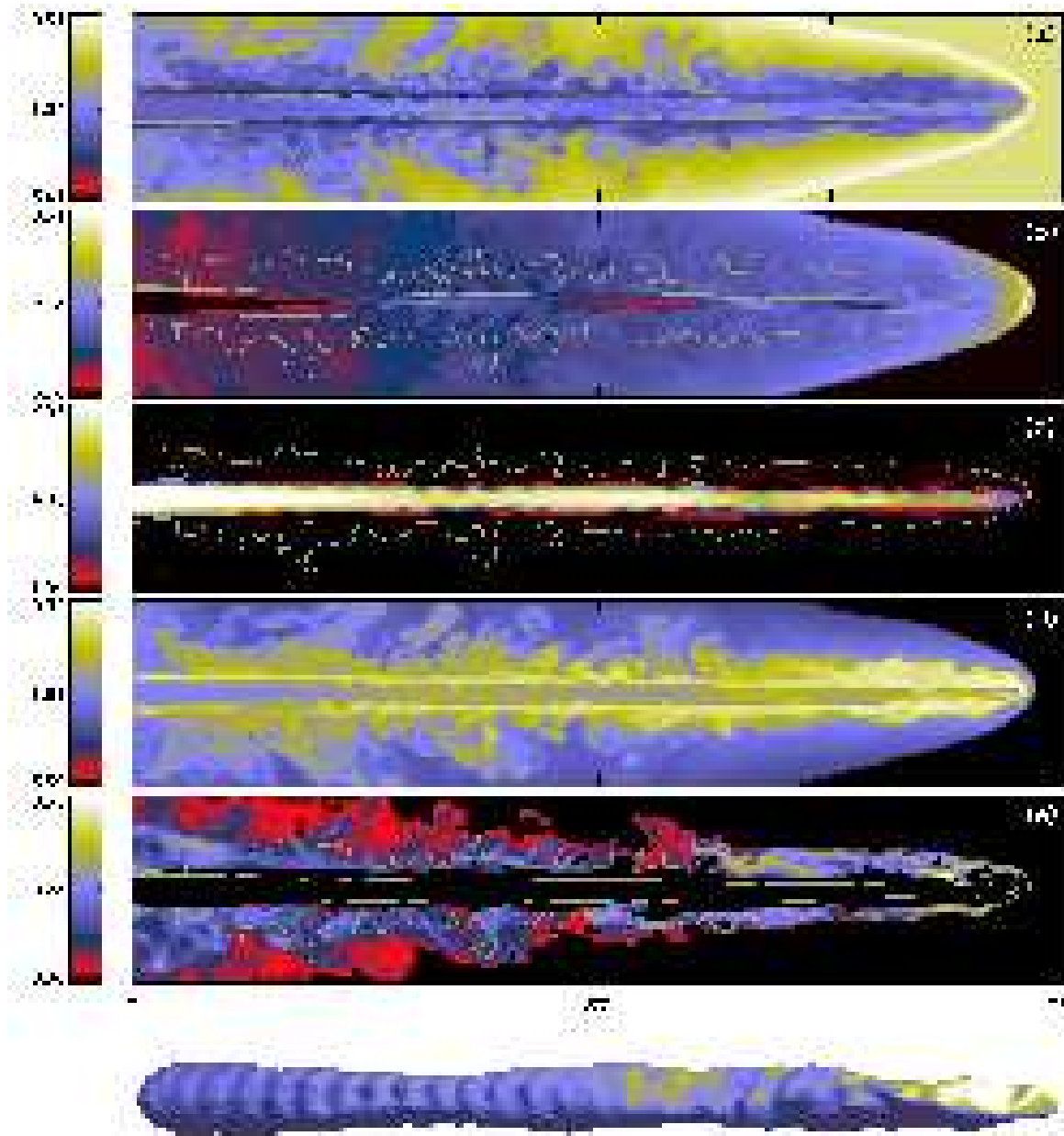


Fig. 1.— Rest-mass density, pressure, flow Lorentz factor, specific internal energy and backflow velocity distributions (from top to bottom) of the model discussed in the text in the plane $y = 0$ at the end of the simulation. White contour levels appearing in each frame correspond to values of f equal to 0.95 (inner contour; representative of the beam) and 0.05 (representative of the cocoon/shocked external medium interface). The bottom panel displays the isosurface of $f = 0.95$.



Fig. 2.— Mean local apparent speed for the jet of Fig. 1 observed at an angle of 40 degrees. Arrows show the projected direction and magnitude of the apparent motion the contours corresponding to values of $1.0c$, $1.6c$, and $2.2c$, respectively. Averages have been computed along the line of sight for each pixel in the image (computational cell) using the emission coefficient as a weight.

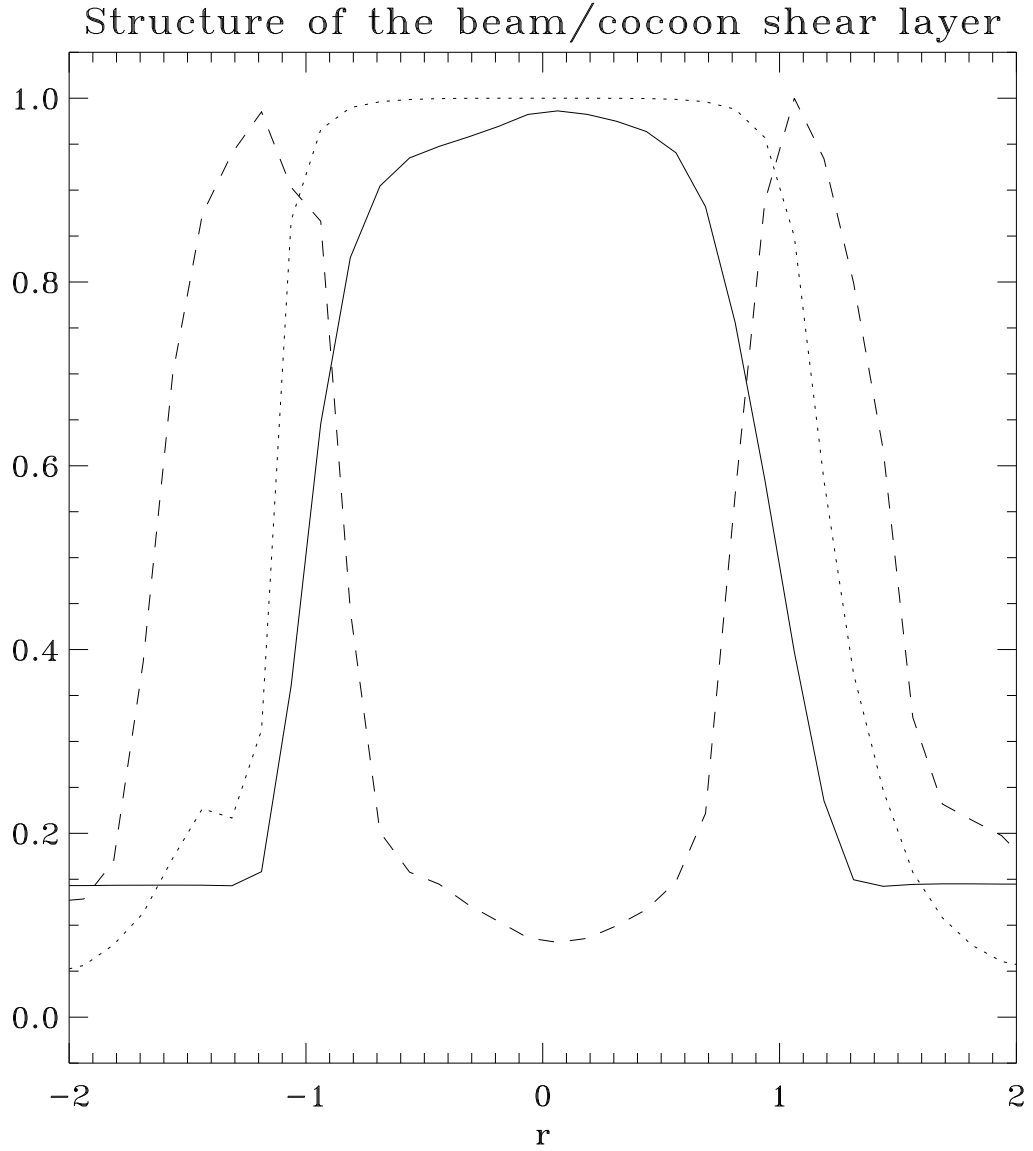


Fig. 3.— Beam mass fraction (dotted line), flow Lorentz factor (filled line) and specific internal energy (dashed line), in arbitrary units, across the beam ($z = 11.7R_b$).

Beam mean radius and axial momentum

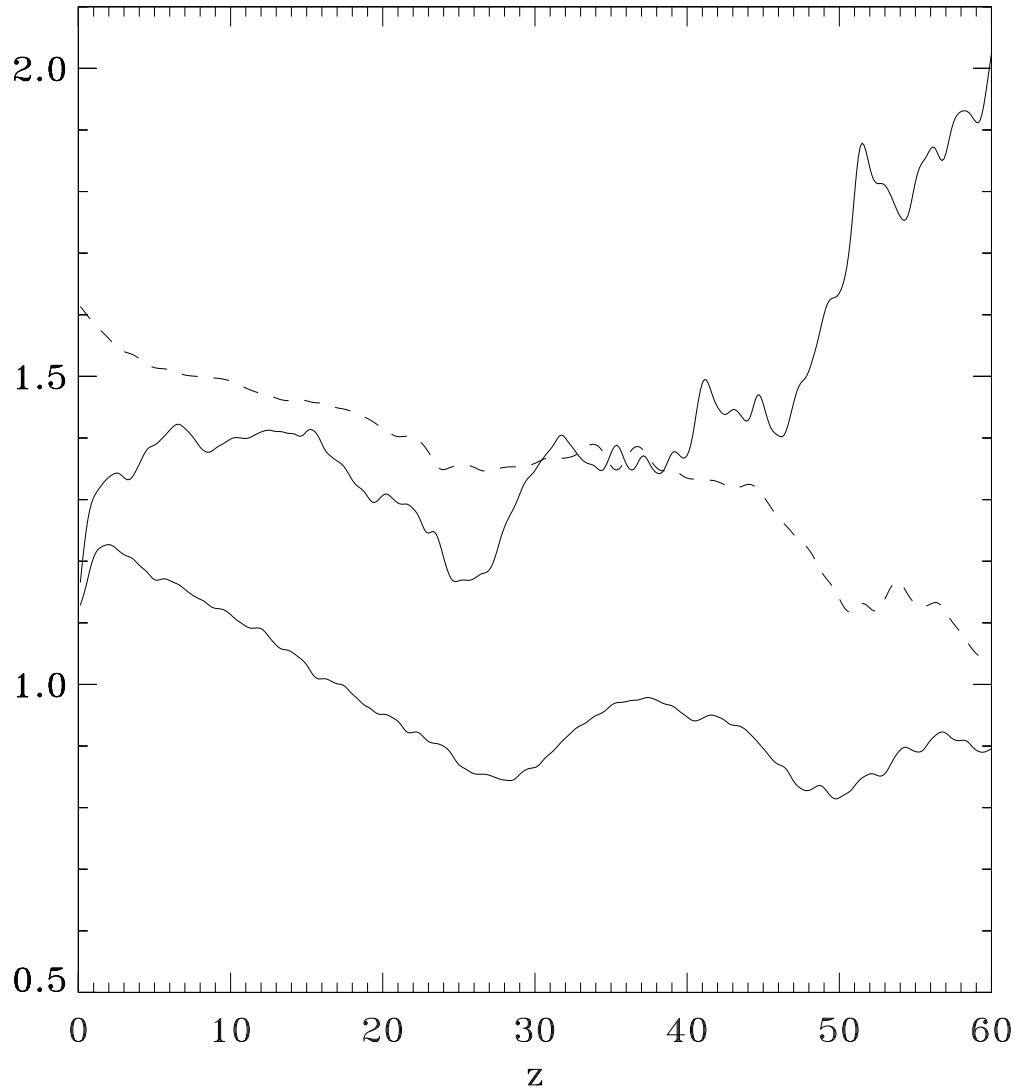


Fig. 4.— Dashed line: Axial component of the momentum of the beam particles (integrated across the beam) along the jet axis at the end of the simulation. Solid lines: Mean beam radius along the axis for $f \geq 0.2$ (top line) and $f \geq 0.8$ (bottom line), respectively. Quantities are in code units.